RSC Advances

ROYAL SOCIETY OF CHEMISTRY

www.rsc.org/advances

Journal Name

RSCPublishing

ARTICLE

Facile fabrication of red phosphorus/TiO_2 composites for lithium ion batteries

Cite this: DOI: 10.1039/x0xx00000x

Han Xiao [1], Yang Xia[1,*], Yongping Gan[1], Hui Huang[1], Chu Liang[1], Xinyong Tao[1], Lusheng Xu[2] and Wenkui Zhang[1,*]

Received 00th January 2012,
Accepted 00th January 2012

DOI: 10.1039/x0xx00000x

www.rsc.org/

Red phosphorus (RP) is an attractive anode material with an ultrahigh specific capacity of 2596 mAh g^{-1}. However, its rapid capacity decay attribute to the volume expansion during the lithiation process presents a noteworthy technical challenge. Meanwhile, titanium oxide (TiO_2) is a good candidate for lithium ion batteries owing to its high safety and outstanding stability, but it is restricted by the low capacity of 167 mAh g^{-1} at room temperature. Inspired by reinforced concrete structure, we fabricate RP built-in amorphous TiO_2 (A-TiO_2) composite in consideration of achieving complementary effects. Herein, A-TiO_2 could act as "concrete" to prevent RP from escaping the electrode. While RP plays the role of "steel", which could improve the electrochemical capacity of composite. As a result, RP/A-TiO_2 composite demonstrates an enhanced cycling capacity of 369 mAh g^{-1} over 100 cycles as well as an acceptable rate capacity of 202 mAh g^{-1} at the current density of 1 A g^{-1}. This designed unique reinforced concrete structure may provide a novel strategy to fabricate high electrochemical performance anodic materials for advanced lithium ion batteries.

1. Introduction

Rechargeable lithium ion batteries (LIBs) are considered as the most promising power sources for emerging portable electric vehicles and renewable power station.[1-6] Massive efforts have been made to develop advanced electrode materials with high power density, long cycle stability, and practical reliability.[7-10] TiO_2 is one of the most attractive anode materials because of its high safety and outstanding stability.[11-14] However, the low theory capacity restricts its application. Fortunately, the remarkable stability during the lithium insertion/extraction processes provides a favourable possibility to composite with other modest anode materials.[15-20] In this aspect, elemental phosphorus is a particularly attractive anode material, which can react with 3 Li atoms to form Li_3P compounds, giving a theoretical specific capacity of 2596 mAh g^{-1}.[21] This ultrahigh capacity makes phosphorus as a good candidate for compositing with TiO_2. Among the three allotropes of phosphorus, white phosphorus is highly toxic and easily oxidized, which is fundamentally unsuitable as an electrode material. While black phosphorus is an alternative anode material in consequence of graphite-like structure and good electrical conductivity.[22, 23] Yet to synthesize black phosphorus, extremely high pressure (1.2 Gpa) is usually needed.[24] Red phosphorus is a suitable allotrope because it is abundant, safe, and chemically stable.[25, 26] Nevertheless, due to its electronic insulation and volume expansion effects, the practical capacity of RP is far from the theoretical value. Recently, Jiang *et al*. reported that nanosized phosphorus hosted in porous carbon composite, which could deliver a highly reversible capacity.[25] However, RP composite with TiO_2 to enhance the electrochemistry capacity has not been reported yet.

Herein, we attempt to design and fabricate RP/A-TiO_2 composites *via* a reinforced concrete structural strategy. On the one hand, RP would greatly increase the power density of RP/A-TiO_2 composite. On the other hand, A-TiO_2 in rational constructed RP/A-TiO_2 could effectively stabilize the RP phase. In comparison with A-TiO_2 and bare RP, RP/A-TiO_2 composite exhibits the intensified capacity in consequence of this unique reinforced concrete structure.

2. Experimental Section

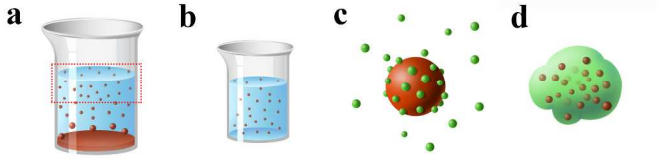

Scheme 1. The preparation and structure illustration of RP (red color)/A-TiO_2 (green color).

2.1 Preparation of samples

2.1.1 Preparation of nanosized red phosphorus

In typical experiment, 20 g commercial RP (98.5%, purity) was processed by high energy ball-milling for 48 hours. The resulting RP powder was then added in 500 ml PVP (K30) aqueous solution (4wt %). The mixed suspension was further treated by using ultrasonic for 2 hours. Afterward, in order to obtain the nanosized RP, the suspension (Scheme 1a) was placed in atmosphere for 48 hours.

2.1.2 Preparation of RP/A-TiO_2

100 ml of suspension contained nanosized RP particles (Scheme 1a) was extracted to prepare RP/A-TiO_2 composite (Scheme 1b). Firstly, 2 g isopropyl titanate was uniformly dispersed into 20 ml ethanol. Then isopropyl titanate solution was slowly dripped into the as prepared RP suspension so that the hydrolyzed titanium dioxide would attach on phosphorus (Scheme 1c). After stirring for 10 minutes, the precipitation was centrifuged and washed for several times. Finally, the sample was dried at 80 ^{o}C in an oven for 12 hours (product is illustrated in Scheme 1d).

2.2 Characterization

The morphology of the product was observed by scanning electron microscopy (SEM, Hitachi S-4700) and transmission electron microscopy (TEM, FEI, Tecnai G2 F30). Powder X-ray diffraction (XRD) was performed using Rigaku Ultima IV with Cu Kα radiation (λ = 0.15418 nm) in the 2θ range from 10-80^{o}. Nitrogen adsorption-desorption was determined by Brunanuer-Emmett-Teller (BET) tests using a Nova 1000e (Quantachrome Instruments) surface area and pore analyzer. The content of RP in RP/A-TiO_2 composite was tested by a thermo gravimetric analyzer (TGA, Q5000IR) in N_2 atmosphere with the heating rate of 10 ^{o}C/min. Fourier transform-infrared spectroscopy (FT-IR) spectrum was characterized on Nicolet 6700.

2.3 Electrochemical Measurements

The electrochemical tests were performed using a coin-type half cell (CR 2025). Active material, acetylene black and polyvinylidene fluoride (PVDF) binder were mixed by the weight ratio of 70: 15: 15 in N-methylpyrrolidone (NMP) as the dispersant. The resultant viscous slurry was cast on copper foil and dried at 120 ^{o}C under vacuum for 12 hours. Cells were assembled in an argon-filled glovebox with the metallic lithium foil as the counter electrode, 1 M $LiPF_6$ in ethylene carbonate (EC)-dimethyl carbonate (DMC) (1:1 in volume) as the electrolyte, and a polypropyle (PP) microporous film (Cellgard 2300) as the separator. The charge-discharge test was carried out on a Neware battery test system in the voltage range of 0.01-3 V at room temperature. A CHI 660b work-station was applied for cyclic voltammograms (CV) tests in the voltage range of 0-3 V at a scan rate of 0.1 mV s^{-1}.

3. Results and discussion

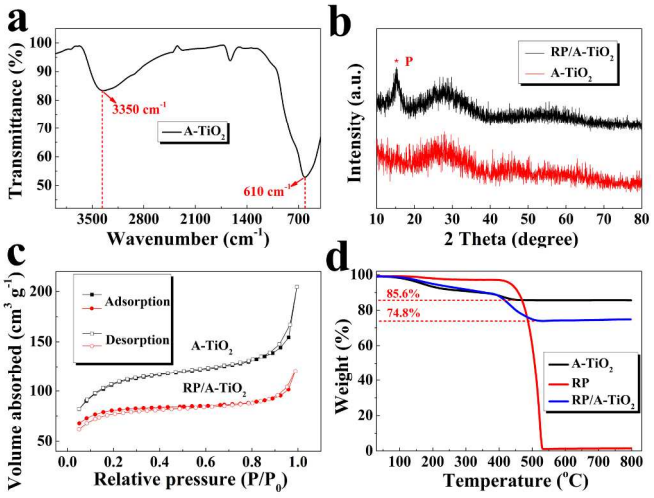

Figure 1. (a) FT-IR spectrum of amorphous TiO_2. (b) XRD patterns of A-TiO_2 and RP/A-TiO_2. (c) Nitrogen (N_2) adsorption-desorption isotherms of A-TiO_2 and RP/A-TiO_2. (d) TGA curves of RP/A-TiO_2

Figure 1a shows FT-IR spectrum of isopropyl titanate hydrolyzate. The broad peak at ~3350 cm^{-1} is corresponding to the surface-adsorbed water and hydroxyl groups.[27] The sharp peak at ~600 cm^{-1} confirms to the absorption of Ti-O bond.[28, 29] The amorphous structure of A-TiO_2 is supported by broad XRD peaks in Figure 1b. The peak around 15^{o} in RP/A-TiO_2 pattern is in agreement with amorphous red phosphorus.[21, 26] Nitrogen (N_2) adsorption-desorption isotherms BET results are depicted in Figure 1c. The BET surface area of A-TiO_2 is identified to be 344.7 m^2 g^{-1}. However, RP/A-TiO_2 sample decreases to 254.2 m^2 g^{-1}, which can be attributed to the built-in RP. Both isotherms are typical type II with an inflection point around 0.2 relative pressure (p/p_o), representing surface adsorption consequence. TGA was carried out to investigate the content of RP in the RP/A-TiO_2 composite under N_2 atmosphere. As shown in Figure 1d, A-TiO_2 shows a weight loss of 14.4% up to 450 ^{o}C, arising from the coordinated water. There is a sharp weight loss about 96% in RP sample ranging from 410 to 530 ^{o}C, which is resulting from the sublimation process. Based on the above results, the weight loss of 15.2% in RP/A-TiO_2 sample is due to both coordinated water and sublimated RP. Thus the content of RP in RP/A-TiO_2 is calculated to be 12.6%.

SEM observations were employed to characterize the morphology of the products. A-TiO_2 sample (figure 2a and b) consists of self-aggregated nanoparticles. Figure 2c and d depict irregular particles of bare RP with a particle size ranging from micrometer to nanometer. In the counterpart (figure 2e and f), RP/A-TiO_2 composite has a rough surface, which is due to the hydrolyzed TiO_2 particles wrap on the surface of RP. As

mentioned in the experimental part, A-TiO_2 nanoparticles are *in-situ* hydrolysed in the preparing process. A part of A-TiO_2 will directly wrap on the surface of RP, while the rest of A-TiO_2 nanoparticles will fill into the interval among the A-TiO_2 coated RP particles since the main component is A-TiO_2 based on the TG results (figure 1d). Therefore the A-TiO_2 coated RP particles will act as "steel", and the dispersed A-TiO_2 nanoparticles will act as "concrete", achieving a unique reinforced concrete structure. Such reinforced concrete model offers a very stable structure, which has the following merits. Firstly, A-TiO_2 plays the role as "concrete", which could provide better feasibility and plasticity to accommodate the volume change of RP particles and avoid the direct contact between RP and electrolyte during Li-insertion/extraction reactions. Secondly, RP particles act as "steel", which will offer high electrochemical capacity and enhance the energy density for the composite. Thus this strategy will improve the structural stability and specific capacity.

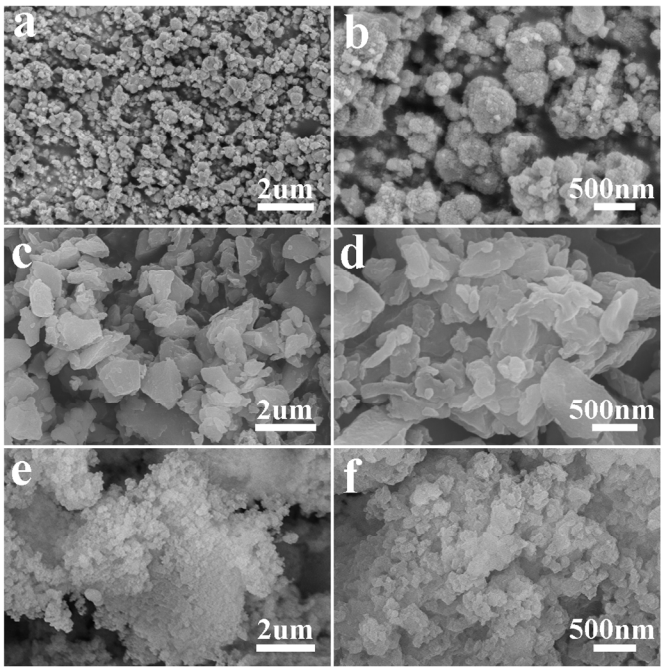

Figure 2. (a and b) SEM images of A-TiO_2; (c and d) SEM images of bare RP; (e and f) SEM images of RP/A-TiO_2.

TEM was utilized to get a deep insight into the detail microstructure. As revealed in figure 3a, the primary particle size of A-TiO_2 cluster is identified to be ~50 nm. In order to further clarify the microstructural differences of three samples, TEM images of bare RP (figure 3c) and RP/A-TiO_2 (figure 3e) were also supplied. Compared with bare RP, RP/A-TiO_2 reveals plenty of nanosized particles (A-TiO_2) wrap on the surface of the inner nanosized particles (RP), matching well with the proposed reinforced concrete model. Figure 3b, d and f represent the high-resolution TEM (HRTEM) images and selected area electron diffraction (SAED) patterns (insert in top right corner) of A-TiO_2, bare RP and RP/A-TiO_2 respectively. HRTEM images obviously show that all the three samples only have disordered lattice fringes, suggesting TiO_2, RP and RP/A-TiO_2 are all amorphous. Moreover, SAED patterns also confirm that all the samples have the poor crystallization, which is consistent well with the XRD results.

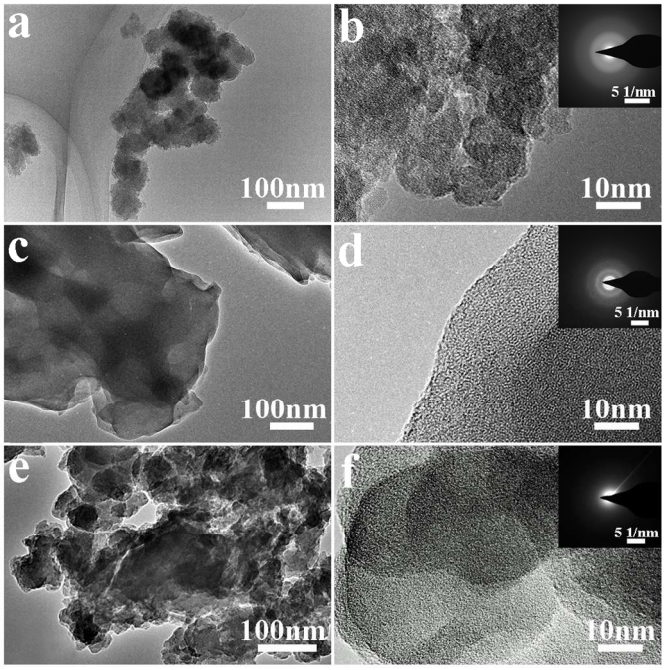

Figure 3. (a and b) TEM and HRTEM images of A-TiO_2; (c and d) TEM and HRTEM images of bare RP; (e and f) TEM and HRTEM images of A-TiO_2/RP; The insert pictures in HRTEM are the corresponding SAED images.

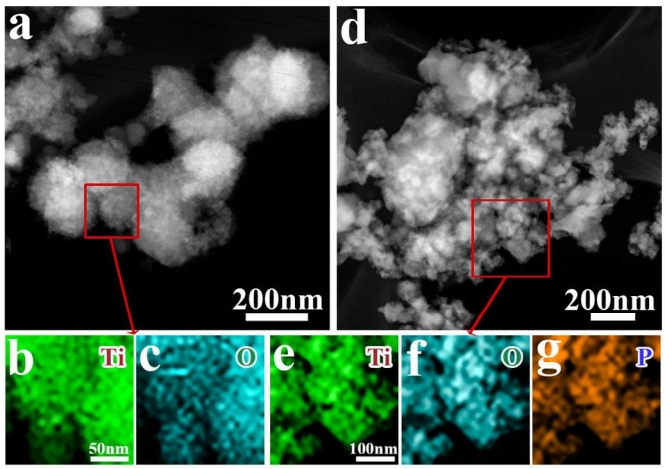

Figure 4. (a) STEM image of A-TiO_2; elemental mappings of titanium (b) and oxygen (c); (d) STEM image of RP/A-TiO_2; elemental mappings of titanium (e), oxygen (f), and phosphorus (g)

To verify the composition of A-TiO_2 and RP/A-TiO_2, scanning transmission electron microscope (STEM) and area-scan elemental mapping images are supplied. Figure 4a-c present the morphology and elements distribution of A-TiO_2. As seen in figure 4a, A-TiO_2 exhibits rough surface, which is similar to the SEM results (figure 2f). Taken from red square

area of A-TiO_2 in figure 4a, the energy-dispersive spectroscopy (EDS) mappings demonstrate titanium element (figure 4b) and oxygen (figure 4c) element are dispersed homogeneously, implying the chemical composition of A-TiO_2. The detailed microstructure and elements mappings of RP/A-TiO_2 sample are showed in figure 4d-g. As seen in figure 4d, mapping square is selected in nanoparticles cluster area. Three elements of titanium (figure 4e), oxygen (figure 4f) and phosphorus (figure 4g) have the uniform distribution, suggesting the *in-situ* formed A-TiO_2 is tightly contacted with RP particles. These results also indicate that RP/A-TiO_2 has the unique reinforced concrete structure.

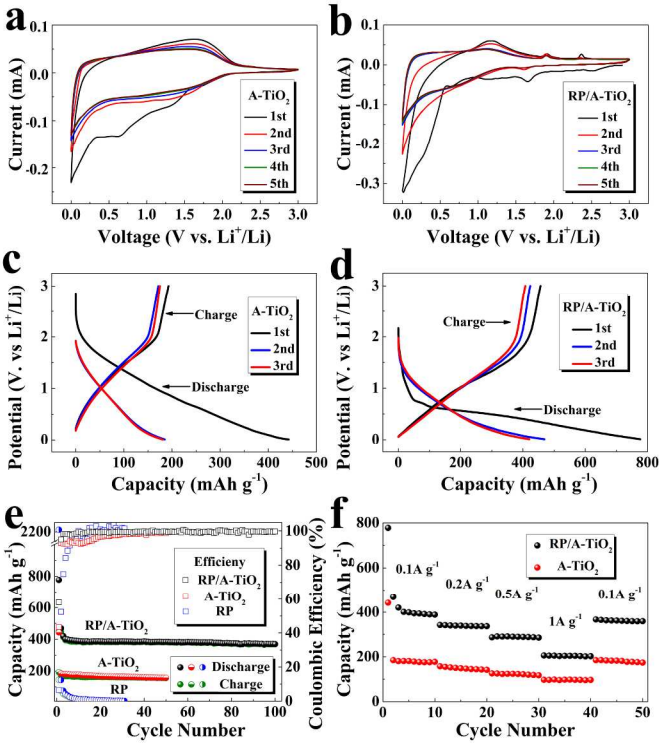

Figure 5. (a and b) CV curves of A-TiO_2 and RP/A-TiO_2, respectively. (c and d) Discharge-charge profiles of A-TiO_2 and RP/A-TiO_2 with a current density of 100 mA g^{-1}, respectively. (e) Cycling performances of A-TiO_2 and RP/A-TiO_2 with a current density of 100 mA g^{-1}. (f) Rate performance of A-TiO_2 and RP/A-TiO_2 electrodes.

Figure 5 depicts the electrochemical performance of A-TiO_2 and RP/A-TiO_2. There is a pair of broad anodic/cathodic peaks in the CV curves of A-TiO_2 (figure 5a), corresponding to the typical lithium insertion/extraction potential of A-TiO_2.[30] Compared with A-TiO_2 sample, the broad redox potential of RP/A-TiO_2 (figure 5b) is lower than A-TiO_2. This result can be attributed to the electrode polarization since the RP has a much poorer electronic conductivity.[31] Moreover, a small anodic peak at ~2.4 V can be seen in the first two cycles, representing some irreversible process. As shown in figure 5c, the first discharge and charge capacities of A-TiO_2 sample are 440 and 180 mAh g^{-1}, respectively. The irreversible capacity loss reaches up to 260 mAh g^{-1}. The sharply dropped capacity loss could be explained by the formation of solid electrolyte interface (SEI) layer[32] and the reaction of H_2O/-OH species adsorbed at the surface of sample[33]. Meanwhile, the first discharge and charge capacities of RP/A-TiO_2 sample are 770 and 450 mAh g^{-1}, which has a larger irreversible capacity loss of 320 mAh g^{-1}. This larger irreversible capacity loss compared with A-TiO_2 could be related to the formation of SEI layer in RP component.[25]

Figure 5e presents the cycling performance of RP, A-TiO_2, and RP/A-TiO_2 samples. As seen in figure 5e, the capacity of bare RP sharply falls from 2222 to 143 mAh g^{-1} in the initial several cycles, and continually fall to 12 mAh g^{-1} at 30th cycle. That exhibits an extremely poor electrochemical performance. However, A-TiO_2 and RP/A-TiO_2 electrodes show the excellent cycling stability. The Coulombic efficiency of A-TiO_2 and RP/A-TiO_2 steadily reaches around 99% accompanied by the cycle number increasing. The discharge capacities of bare RP (30th), A-TiO_2 (50th) and RP/A-TiO_2 (100th) are 12, 157 and 369 mAh g^{-1}, corresponding to 21.1, 93.4 and 89.3% capacity retentions of their initial discharge capacities (here we use the 3rd cycle data because the discharge capacity is becoming stable) of 57, 167 and 413 mAh g^{-1}, respectively. It is note that the capacity retention of RP/A-TiO_2 at 50th reaches to 92.3%, which is comparable with the A-TiO_2 result of 93.4%. However, RP/ A-TiO_2 shows a much higher capacity retention of 369 mAh g^{-1} compared with bare RP and A-TiO_2. Figure 5f displays the rate performance of A-TiO_2 and RP/A-TiO_2 at various rates current densities. The discharge capacities of A-TiO_2 and RP/A-TiO_2 are reserved at 388/177, 336/141, 285/117, and 202/97 mAh g^{-1} at the current densities of 100, 200, 500 and 1000 mA g^{-1}, respectively. It is noticed that the capacities at higher currents faded rapidly. However, when the current is restored to 100 mA g^{-1}, A-TiO_2 and RP/A-TiO_2 both deliver the reversible capacity of 359 and 174 mAh g^{-1}, respectively. This phenomenon is mainly due to the kinetic-limited effects of the electrochemical reaction in nature, rendering a higher over potential and a lower capacity at a higher current.[34] Obviously, RP/A-TiO_2 composite has a high reversible capacity and stable cycling performance that is mainly attributed to the unique with reinforced concrete structure. On the one hand, A-TiO_2 stores lithium by addition-type reaction ($xLi^+ + TiO_2 + xe^- \rightarrow Li_xTiO_2$)[30], which has a remarkable structural stability. It also can prevent the continuous capacity loss of RP derived from the crack and pulverization. On the other hand, RP has a large capacity in nature, which could provide more reversible capacity for the RP/A-TiO_2 composite.

Since RP is extremely unstable during the Li^+ insertion/extraction, we do the comparison of fresh and cycled RP/A-TiO_2 electrode *via* STEM and area-scan elemental mapping tests to clarify the structural stability directly. Figure

6a and f clearly present the STEM image of fresh RP/A-TiO_2 electrode. Combining with elemental mapping analysis, P, Ti and O (figure 6b-d) are well dispersed in the acetylene black (figure 6e). For the cycled counterpart, the electrode was charged to 3V (lithium extraction status) after 100 cycles. Elemental mappings in figure 6f-j reveal that the RP is distributed in the electrode as uniform as the fresh one. Figure 6k illustrates the working principle of RP/A-TiO_2 with reinforced concrete structure during the charge-discharge processes. When the expansion of inner RP occurs, the outer TiO_2 cluster could buffer flexibly, preventing the RP running off. By effectively use the inner RP, 10 wt% RP could supply more than 200 mAh g^{-1} capacity in the composite, which render the double capacity comparing with A-TiO_2.

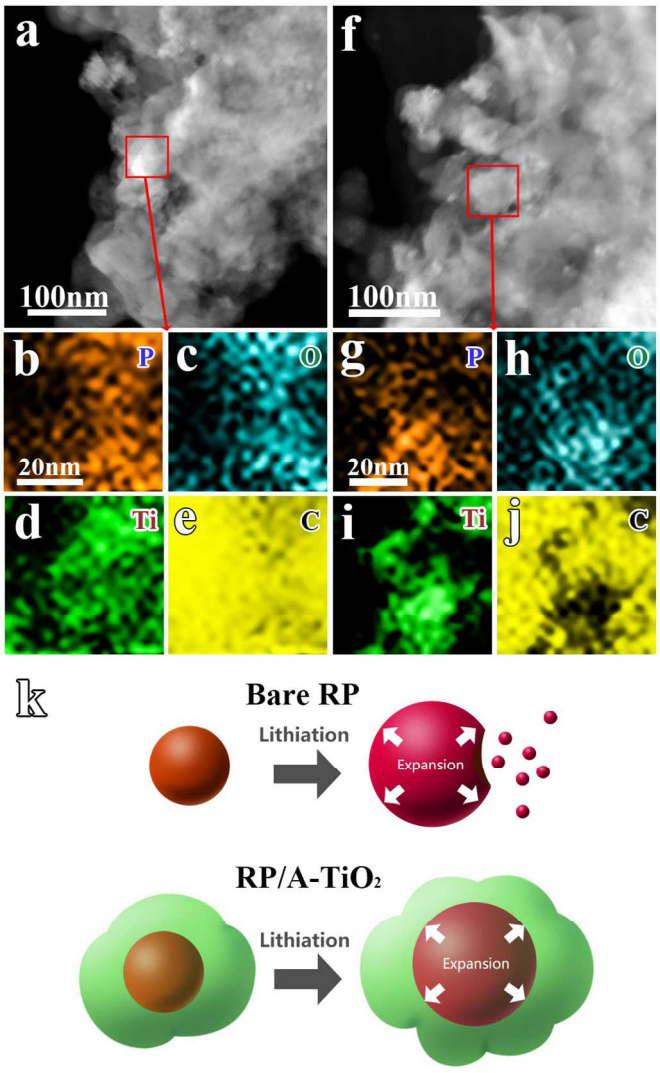

Figure 6. (a) STEM image of RP/A-TiO_2 electrode before cycling; (b-e) area-scan elemental mapping images of red square area in figure 6 a. (f) STEM image of RP/A-TiO_2 electrode after cycling; (g-j) area-scan elemental mapping images of red square area in figure 6 f. (k) Schematic of lithiation process in bare RP and RP/A-TiO_2.

4. Conclusions

In summary, a novel RP/A-TiO_2 composite with the unique reinforced concrete structure was synthesized by *in-situ* hydrolyzing on RP particles. RP and A-TiO_2 play as the roles of "reinforced" and "concrete" respectively. Due to the synergistic effect of RP and A-TiO_2, the as-prepared RP/A-TiO_2 composite not only offers an enhanced reversible capacity, but also keeps the structural stability, presenting the remarkable electrochemical performance (369 mAh g^{-1}, 100 cycles). Therefore, such a RP/A-TiO_2 composite is a very promising anode material for advanced LIBs.

Acknowledgements

This work was supported by National Natural Science Foundation of China (51201151, 51172205 and 201403196), Natural Science Foundation of Zhejiang Province (LR13E020002 and LY13E020010), Scientific Research Foundation of Zhejiang Provincial Education Department (Y201432424) and New Century Excellent Talents in University (NCET 111079).

Notes and references

1 College of Materials Science and Engineering, Zhejiang University of Technology, Hangzhou, 310014, China.
E-mail: nanoshine@zjut.edu.cn (Y. Xia), msechem@zjut.edu.cn (W.K. Zhang); Tel: +86-571-88320394
2 College of Biological and Environmental Engineering, Zhejiang University of Technology, Hangzhou, 310014, China.

1. V. Etacheri, J. E. Yourey and B. M. Bartlett, *Acs Nano*, 2014, **8**, 1491-1499.
2. R. W. Mo, Z. Y. Lei, K. N. Sun and D. Rooney, *Adv Mater*, 2014, **26**, 2084-2088.
3. A. Attia, Q. Wang, X. K. Huang and Y. Yang, *J Solid State Electr*, 2012, **16**, 1461-1471.
4. M. Armand and J. M. Tarascon, *Nature*, 2008, **451**, 652-657.
5. B. Kang and G. Ceder, *Nature*, 2009, **458**, 190-193.
6. A. S. Arico, P. Bruce, B. Scrosati, J. M. Tarascon and W. Van Schalkwijk, *Nat Mater*, 2005, **4**, 366-377.
7. H. Huang, W. J. Zhu, X. Y. Tao, Y. Xia, Z. Y. Yu, J. W. Fang, Y. P. Gan and W. K. Zhang, *Acs Appl Mater Inter*, 2012, **4**, 5974-5980.
8. X. Y. Tao, J. T. Zhang, Y. Xia, H. Huang, J. Du, H. Xiao, W. K. Zhang and Y. P. Gan, *J Mater Chem A*, 2014, **2**, 2290-2296.
9. Y. Xia, W. K. Zhang, Z. Xiao, H. Huang, H. J. Zeng, X. R. Chen, F. Chen, Y. P. Gan and X. Y. Tao, *J Mater Chem*, 2012, **22**, 9209-9215.
10. S. B. Yang, X. L. Feng, S. Ivanovici and K. Mullen, *Angew Chem Int Edit*, 2010, **49**, 8408-8411.
11. H. Huang, J. W. Fang, Y. Xia, X. Y. Tao, Y. P. Gan, J. Du, W. J. Zhu and W. K. Zhang, *J Mater Chem A*, 2013, **1**, 2495-2500.
12. X. Zhang, H. X. Chen, Y. P. Xie and J. X. Guo, *J Mater Chem A*, 2014, **2**, 3912-3918.
13. S. H. Choi, J. H. Lee and Y. C. Kang, *Nanoscale*, 2013, **5**, 12645-12650.
14. H. T. Fang, M. Liu, D. W. Wang, T. Sun, D. S. Guan, F. Li, J. G. Zhou, T. K. Sham and H. M. Cheng, *Nanotechnology*, 2009, **20**.

15. J. S. Chen, D. Y. Luan, C. M. Li, F. Y. C. Boey, S. Z. Qiao and X. W. Lou, *Chem Commun*, 2010, **46**, 8252-8254.
16. Y. P. Tang, D. Q. Wu, S. Chen, F. Zhang, J. P. Jia and X. L. Feng, *Energ Environ Sci*, 2013, **6**, 2447-2451.
17. X. Y. Li, Y. M. Chen, L. M. Zhou, Y. W. Mai and H. T. Huang, *J Mater Chem A*, 2014, **2**, 3875-3880.
18. L. Yu, Z. Y. Wang, L. Zhang, H. B. Wu and X. W. Lou, *J Mater Chem A*, 2013, **1**, 122-127.
19. D. S. Guan, J. Y. Li, X. F. Gao and C. Yuan, *J Power Sources*, 2014, **246**, 305-312.
20. C. M. Ban, M. Xie, X. Sun, J. J. Travis, G. K. Wang, H. T. Sun, A. C. Dillon, J. Lian and S. M. George, *Nanotechnology*, 2013, **24**.
21. J. F. Qian, D. Qiao, X. P. Ai, Y. L. Cao and H. X. Yang, *Chem Commun*, 2012, **48**, 8931-8933.
22. L. Q. Sun, M. J. Li, K. Sun, S. H. Yu, R. S. Wang and H. M. Xie, *J Phys Chem C*, 2012, **116**, 14772-14779.
23. M. Nagao, A. Hayashi and M. Tatsumisago, *J Power Sources*, 2011, **196**, 6902-6905.
24. C. M. Park and H. J. Sohn, *Adv Mater*, 2007, **19**, 2465-+.
25. L. Wang, X. M. He, J. J. Li, W. T. Sun, J. Gao, J. W. Guo and C. Y. Jiang, *Angew Chem Int Edit*, 2012, **51**, 9034-9037.
26. Y. Kim, Y. Park, A. Choi, N. S. Choi, J. Kim, J. Lee, J. H. Ryu, S. M. Oh and K. T. Lee, *Adv Mater*, 2013, **25**, 3045-3049.
27. X. F. Wang and L. Andrews, *J Phys Chem A*, 2005, **109**, 10689-10701.
28. Z. Liu, Z. C. Jian, J. Z. Fang, X. X. Xu, X. M. Zhu and S. X. Wu, *Int J Photoenergy*, 2012.
29. J. Fang, F. Wang, K. Qian, H. Z. Bao, Z. Q. Jiang and W. X. Huang, *J Phys Chem C*, 2008, **112**, 18150-18156.
30. Y. M. Lin, P. R. Abel, D. W. Flaherty, J. Wu, K. J. Stevenson, A. Heller and C. B. Mullins, *J Phys Chem C*, 2011, **115**, 2585-2591.
31. G. Jeong, J. H. Kim, Y. U. Kim and Y. J. Kim, *J Mater Chem*, 2012, **22**, 7999-8004.
32. C. Marino, L. Boulet, P. Gaveau, B. Fraisse and L. Monconduit, *J Mater Chem*, 2012, **22**, 22713-22720.
33. W. J. H. Borghols, D. Lutzenkirchen-Hecht, U. Haake, W. Chan, U. Lafont, E. M. Kelder, E. R. H. van Eck, A. P. M. Kentgens, F. M. Mulder and M. Wagemaker, *J Electrochem Soc*, 2010, **157**, A582-A588.
34. Y. Xia, Z. Xiao, X. Dou, H. Huang, X. H. Lu, R. J. Yan, Y. P. Gan, W. J. Zhu, J. P. Tu, W. K. Zhang and X. Y. Tao, *Acs Nano*, 2013, **7**, 7083-7092.